New Journal of Physics
The open access journal at the forefront of physics

Deutsche Physikalische Gesellschaft DPG IOP Institute of Physics

PAPER • OPEN ACCESS

Transition from electromagnetically induced transparency to Autler–Townes splitting in cold cesium atoms

To cite this article: Liping Hao *et al* 2018 *New J. Phys.* **20** 073024

New Journal of Physics
The open access journal at the forefront of physics

Deutsche Physikalische Gesellschaft DPG
IOP Institute of Physics

Published in partnership with: Deutsche Physikalische Gesellschaft and the Institute of Physics

OPEN ACCESS

RECEIVED
19 March 2018

REVISED
11 June 2018

ACCEPTED FOR PUBLICATION
5 July 2018

PUBLISHED
17 July 2018

PAPER

Transition from electromagnetically induced transparency to Autler–Townes splitting in cold cesium atoms

Liping Hao[1], **Yuechun Jiao**[1,2], **Yongmei Xue**[1], **Xiaoxuan Han**[1], **Suying Bai**[1], **Jianming Zhao**[1,2,4] **and Georg Raithel**[1,3]

[1] State Key Laboratory of Quantum Optics and Quantum Optics Devices, Laser spectroscopy Laboratory, Shanxi University, Taiyuan 030006, People's Republic of China
[2] Collaborative Innovation Center of Extreme Optics, Shanxi University, Taiyuan 030006, People's Republic of China
[3] Department of Physics, University of Michigan, Ann Arbor, MI 48109-1120, United States of America
[4] Author to whom any correspondence should be addressed.

E-mail: zhaojm@sxu.edu.cn

Keywords: Rydberg-EIT, Autler–Townes splitting, cascade three-level atom

Abstract

Electromagnetically induced transparency (EIT) and Autler–Townes splitting (ATS) are two similar yet distinct phenomena that modify the transmission of a weak probe field through an absorption medium in the presence of a coupling field, featured in a variety of three-level atomic systems. In many applications it is important to distinguish EIT from ATS splitting. We present EIT and ATS spectra in a three-level cascade system, involving cold cesium atoms in the $35S_{1/2}$ Rydberg state. The EIT linewidth, $\gamma_{\rm EIT}$, defined as the full width at half maximum of the transparency window, and the ATS splitting, $\gamma_{\rm ATS}$, defined as the peak-to-peak distance between AT absorption peaks, are used to delineate the EIT and ATS regimes and to characterize the transition between the regimes. In the cold-atom medium, in the weak-coupler (EIT) regime $\gamma_{\rm EIT} \approx A + B(\Omega_c^2 + \Omega_p^2)/\Gamma_{eg}$, where Ω_c and Ω_p are the coupler and probe Rabi frequencies, Γ_{eg} is the spontaneous decay rate of the intermediate $6P_{3/2}$ level, and parameters A and B that depend on the laser linewidth. We explore the transition into the strong-coupler (ATS) regime, which is characterized by the relation $\gamma_{\rm ATS} \approx \Omega_c$. The experiments are in agreement with numerical solutions of the Master equation. Our analysis accounts for non-ideal conditions that exist in typical realizations of Rydberg-EIT, including laser-frequency jitter, Doppler mismatch of the utilized two-color Rydberg EIT system, and strong probe fields. The obtained criteria to distinguish cold-atom EIT from ATS are readily accessible and applicable in practical implementations.

1. Introduction

Electromagnetically induced transparency (EIT) [1] is a quantum interference effect in which the absorption of a weak probe laser, interacting resonantly with an atomic transition, is reduced in the presence of a coupling laser, which (near-)resonantly couples the upper probe level to a third level. EIT is, for instance, crucial in optically controlled slowing of light [2] and optical storage [3]. Autler–Townes splitting (ATS) [4], proposed by Autler and Townes, is a linear (resonant) AC Stark effect in a two-level system that is strongly driven at resonance, and can be measured via a weak probe from a third level. ATS was observed originally in the microwave and later the light domain. EIT and ATS have been extensively investigated experimentally and theoretically in $\Lambda-$, $V-$ and cascade-type three-level atoms [1, 5–10].

EIT and ATS may phenomenologically look similar, but they are different in nature, one being a quantum interference and the other a linear AC Stark effect. This leads to an interest in the establishment of criteria to discern them. In [9], threshold values for distinguishing EIT and ATS, Ω_t, are defined via the coherence decay rates in the Master equation of the various systems, according to which ATS is observed in four different three-level systems in a strong-coupling-field regime ($\Omega_c / \Omega_t > 1$), whereas EIT is observed only in Λ- and cascade EIT

configurations in a weak-coupling-field regime ($\Omega_c/\Omega_t < 1$). Anisimov *et al* [10] also propose an objective method based on Akaike's information criterion (AIC), to discern ATS from EIT in experimental data of a Λ-type three-level atom. Recently, a series of experiments [11–13] has been performed in which the AIC has been used to discriminate EIT from ATS in Λ-type three-level systems free of Doppler effects. Zhang *et al* [14] provided a theoretical model using a five-level system and investigated EIT and ATS based on the AIC. Another area of interest, in which EIT and ATS are important, is spectroscopy of highly exited Rydberg levels using all-optical methods. Rydberg-EIT, a cascade EIT case, was first observed in a vapor cell [15] and later in a rubidium MOT [16]. In Rydberg-EIT work, the phenomena under investigation are often due to strong Rydberg-atom interactions that are distinct from the optical couplings that give rise to EIT or ATS. For instance, Rydberg-EIT has been used to realize a single-photon transistor [17] and a single-photon source [18, 19] by employing a blockade effect [20–22], which results from the strong Rydberg-atom interactions. ATS has also been investigated in systems that have involved Rydberg states of rubidium [23, 24] and cesium [25, 26]. Exploiting the fact that Rydberg atoms strongly couple to radio-frequency (RF) fields, Rydberg EIT and ATS effects are used to realize precise measurements of such fields [27–31]. Holloway *et al* [32] have investigated the relationship between the Rabi frequency of resonant RF transitions between Rydberg states and the resultant ATS splitting in Rydberg-EIT spectra measured in room-temperature atomic vapor. In related work, the enhancement and suppression of multi-wave mixing (MWM) in five-level systems [33] has been studied, and the effect of Rydberg-atom interactions was explored [34]. Spectra and spatial images of probe and MWM signals were obtained for six-wave [35] and eight-wave implementations [36]. The role of Rydberg interactions as well as the co-occurrence of Rydberg-EIT and ATS were discussed in these works.

While numerous efforts have already dealt with discriminating EIT from ATS [9–14], as reported in the above overview, many of these earlier works are limited to Λ-type systems, deal with Doppler-effect-free cold-atom systems or all-optical equivalents of those, assume that the probe is in the weak-field limit, assume that the system is in steady-state, assume a vanishing laser linewidth, and/or assume that there is no interaction between the atoms (or their analogs) that exhibit EIT or ATS. In the present work we explore the EIT/ATS transition in a case where none of these ideal conditions are necessarily satisfied. We use cascade EIT and ATS, with a Rydberg upper-level state, in a cesium magneto-optical trap (MOT) as an experimental test system. We introduce two parameters, the Rydberg-EIT linewidth, $\gamma_{\rm EIT}$, and the AT spilitting, $\gamma_{\rm ATS}$, to characterize the EIT to ATS transition. In our model, we calculate spectra using methods provided in [32] to study the dependence of $\gamma_{\rm EIT}$ and $\gamma_{\rm ATS}$ on the Rabi frequencies of both the probe and coupling transitions. The transition between EIT and ATS effect is linked to a qualitative change in behavior of $\gamma_{\rm EIT}$ and $\gamma_{\rm ATS}$ as a function of coupler and probe Rabi frequencies. In our analysis, we expand the above cited previous studies to a cascade Rydberg EIT/ATS system. In the numerical methods used, we do not make any weak-field approximations. Also, the Doppler effect, residual Doppler mismatch, averaging over the Maxwell velocity distribution, and inhomogeneous broadening due to laser-frequency jitter are accounted for. The model does not include Rydberg-atom interactions, which are not relevant under the conditions (Rydberg quantum numbers, atom densities and interaction times) used in the experiment. We obtain readily accessible criteria to distinguish EIT from ATS.

2. Theoretical model

We consider the cesium cascade three-level system shown in figure 1(a). The coupling laser drives the upper transition, $|6P_{3/2}, F' = 5\rangle$ ($|2\rangle$) $\rightarrow$$|35S_{1/2}\rangle$ ($|3\rangle$). The weak probe laser couples the lower transition, $|6S_{1/2}, F = 4\rangle$ ($|1\rangle$) $\rightarrow$$|6P_{3/2}, F' = 5\rangle$ ($|2\rangle$). The respective wavelengths and Rabi frequencies are λ_c and Ω_c, and λ_p and Ω_p. In the rotating-wave approximation and the field picture, the Hamiltonian of the three-level atom represented in the space $\{|1\rangle, |2\rangle, |3\rangle\}$ is

$$H = \frac{\hbar}{2}\begin{pmatrix} 0 & \Omega_p & 0 \\ \Omega_p & -2\Delta_p & \Omega_c \\ 0 & \Omega_c & -2(\Delta_p + \Delta_c) \end{pmatrix}, \tag{1}$$

where Δ_c and Δ_p are the detunings of the coupling and probe beams, respectively. To account for decay and dephasing, the system is described using the Lindblad equation for the density matrix ρ

$$\dot{\rho} = -\frac{\mathrm{i}}{\hbar}[H, \rho] + \mathfrak{L}, \tag{2}$$

where $\mathfrak{L}$ is the Lindblad operator that accounts for the decay processes in the atom. In the space $\{|1\rangle, |2\rangle, |3\rangle\}$, $\mathfrak{L}$ becomes [37]

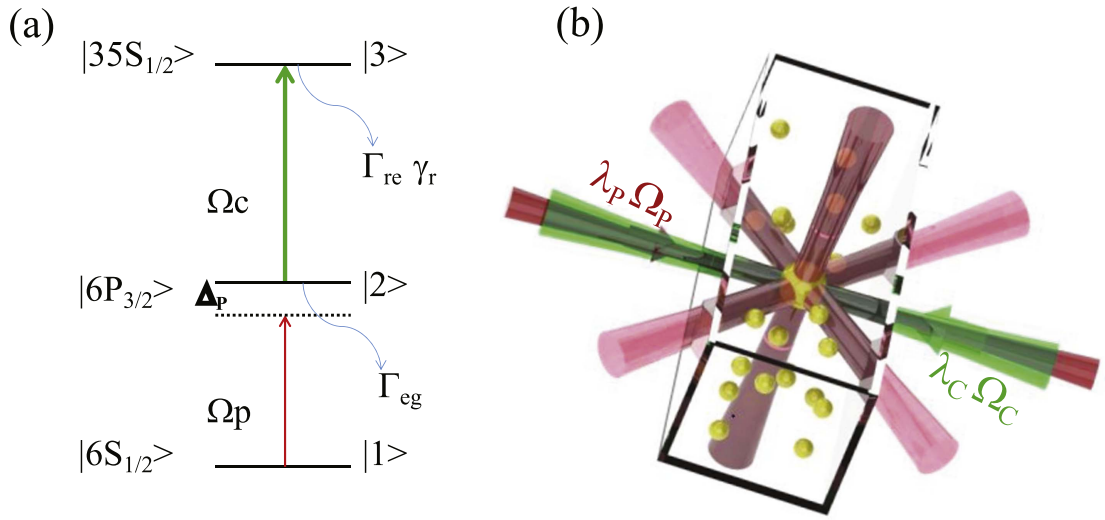

Figure 1. (a) Scheme of the cascade three-level atom. The coupling laser is resonant with the Rydberg transition, $|6P_{3/2}, F' = 5\rangle$ ($|2\rangle$) $\rightarrow$ $|35S_{1/2}\rangle$ ($|3\rangle$) (wavelength 510 nm, Rabi frequency Ω_c). The weak probe beam (wavelength 852 nm, Rabi frequency Ω_p) is referenced to the transition $|6S_{1/2}, F = 4\rangle$ ($|1\rangle$) $\rightarrow$ $|6P_{3/2}, F' = 5\rangle$ ($|2\rangle$) using a Doppler-free polarization spectroscopy setup, and is scanned over the resonance. (b) Sketch of the experimental setup. The laser beams are separated via a dichroic mirror (not shown), and the probe light is detected using a single-photon counter module (SPCM).

$$\mathfrak{L} = \begin{pmatrix} \Gamma_{eg}\rho_{22} & -\frac{1}{2}\gamma_2\rho_{12} & -\frac{1}{2}\gamma_3\rho_{13} \\ -\frac{1}{2}\gamma_2\rho_{21} & -\Gamma_{eg}\rho_{22} + \Gamma_{re}\rho_{33} & -\frac{1}{2}(\gamma_2+\gamma_3)\rho_{23} \\ -\frac{1}{2}\gamma_3\rho_{31} & -\frac{1}{2}(\gamma_2+\gamma_3)\rho_{32} & -\Gamma_{re}\rho_{33} \end{pmatrix}, \tag{3}$$

where γ_2 and γ_3 are the dephasing rates of the intermediate and Rydberg states, respectively. It is $\gamma_2 = \gamma_e + \Gamma_{eg}$, where γ_e is a collision-induced dephasing rate of level $|2\rangle$, and $\gamma_e \ll \Gamma_{eg} = 2\pi \times 5.2$ MHz. Further, $\gamma_3 = \gamma_r + \Gamma_{re}$. For the Rydberg level the population decay rate Γ_{re} is, typically, smaller than the dephasing γ_r, because Rydberg-atom lifetimes are long (lifetimes are $\sim n^3$ and on the order of 100 μs) and interactions between Rydberg atoms in cold-atom clouds are often strong (van der Waals interactions scale as n^{11}).

The spectrum is given by the probe-power transmission, $P = P_0 \exp(-\alpha L)$, with the probe-laser absorption coefficient, $\alpha = 2\pi \mathrm{Im}(\chi)/\lambda_p$, the MOT size, L, and the susceptibility of the medium seen by the probe laser, χ. The susceptibility, χ, is

$$\chi = \frac{2N\mu_{12}}{E_p \epsilon_0}\rho_{12}, \tag{4}$$

where N is the average atomic density, μ_{12} is the dipole moment of transition $|1\rangle \rightarrow |2\rangle$, E_p is the amplitude of the probe, ϵ_0 is the vacuum permittivity, and ρ_{12} is the density matrix element between $|1\rangle$ and $|2\rangle$.

We numerically solve the equations (1)–(3) to obtain the absorption coefficient α for a range of values of Ω_c and Ω_p, including the case of a strong probe, $\Omega_p \gtrsim \Gamma_{eg}$. The result is averaged over the thermal velocity distribution in the gas [32]; under our conditions ($T = 100$–200 μK) the thermal motion is marginally important. In the calculation we also assume $\gamma_r = 0$, which is admissible due to our very low experimental probe intensities and the low principal quantum number of the utilized Rydberg state. Further, in our initial discussion we assume zero laser linewidth; this assumption is dropped later-on.

In figure 2(a) we show α as a function of Ω_c and Δ_p, for the case of a fixed $\Omega_p = 2\pi \times 1.05$ MHz and $\Delta_c = 0$. The shape of the spectrum clearly indicates two qualitatively different regimes, a regime of low Ω_c in which the overall linewidth is fixed at $\approx\Gamma_{eg}$ and there is a very narrow transparency window whose width scales quadratically in Ω_c. This regime is the EIT regime. As Ω_c increases, the overall linewidth increases and the system enters the ATS regime. There, the line breaks up into two features that are narrower than the coupler-free absorption line and the peak-to-peak separation scales linearly in Ω_c. The wide transparency region between the AT lines is almost as wide as the peak-to-peak separation itself.

For a quantitative analysis, we extract the full width at half maximum (FWHM) of the dip in the absorption, γ_{EIT}, as well as the peak-to-peak spacing of the line pair, γ_{ATS}, from the absorption coefficient data. Both parameters γ_{EIT} and γ_{ATS} can be calculated in both the EIT and the ATS regime. However, as detailed in the following, γ_{ATS} yields little useful information in the EIT regime and vice versa. In figure 2(b), both parameters

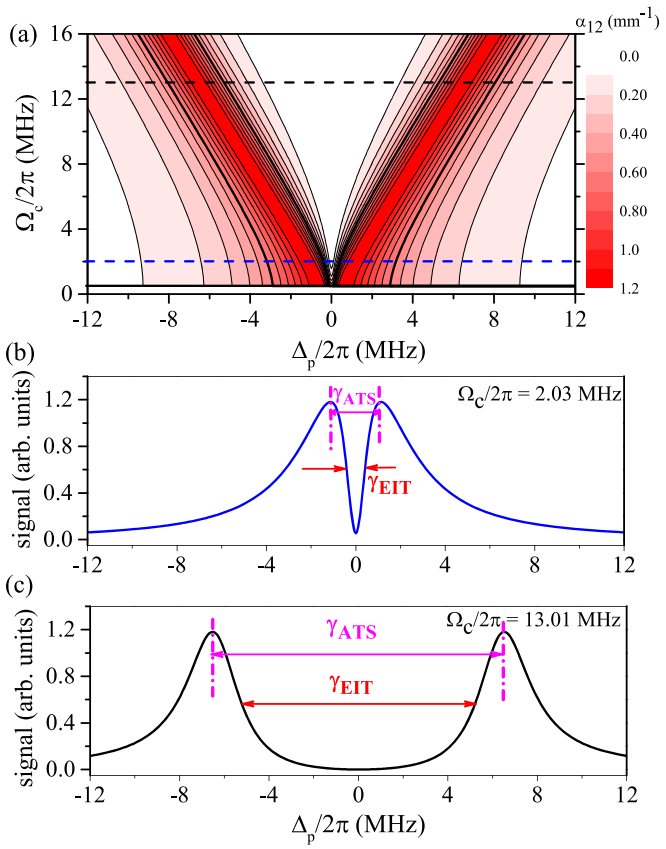

Figure 2. (a) Calculation of the probe absorption coefficient of cold cesium atoms in a MOT, α, for Ω_c ranging from $2\pi \times 0.5$ MHz to $2\pi \times 16$ MHz. The cuts along the horizontal dashed lines correspond to the spectra shown in (b) and (c). (b) Probe absorption coefficient for $\Omega_p = 2\pi \times 1.05$ MHz and $\Omega_c = 2\pi \times 2.03$ MHz, atom density 10^{10} cm^{-3}, and vanishing laser linewidth. This case is in the EIT regime. The FHWM of the EIT window, $\gamma_{\rm EIT}$, and the ATS, $\gamma_{\rm ATS}$, are defined as shown. (c) Same as (b), but for $\Omega_c = 2\pi \times 13.01$ MHz. This case is in the AT regime.

are shown for a typical spectrum in the EIT regime, where $\Omega_p \lesssim \Omega_c = 2\pi \times 2.03$ MHz $< \Gamma_{eg}$. In EIT, the main interest lies in how narrow the EIT transparency window is, in comparison with the natural linewidth Γ_{eg}. Therefore, in the EIT regime the parameter $\gamma_{\rm EIT}$ is most important (hence the name); it measures the bandwidth over which the EIT quantum interference mechanism leading to reduced probe absorption is experimentally observable. In the EIT regime, the separation between the absorption maxima, $\gamma_{\rm ATS}$, carries little useful information, as it just returns a value on the order of the overall coupler-free linewidth. Figure 2(c) shows the spectrum calculated for $\Omega_c = 2\pi \times 13.01$ MHz $> \Gamma_{eg}$, which is the ATS regime. Since ATS is a linear AC Stark effect, the interest mainly is in how far the AT-split line centers are separated from each other. Therefore, in the ATS regime a better parameter to quantify the behavior is the peak-to-peak spacing of the line pair, $\gamma_{\rm ATS}$. As seen in figures 2(a) and (c), in the weak probe limit and for $\Delta_c = 0$, in the ATS regime the peaks tend to have a width of $\Gamma_{eg}/2 = 2\pi \times 2.6$ MHz, and a spacing $\gamma_{\rm ATS} \approx \Omega_c$. (The Rydberg states are very long-lived ($\Gamma_{re} \ll \Gamma_{eg}$) and do not contribute to the width of the AT peaks here).

Figure 3(a) shows the calculated $\gamma_{\rm EIT}$ as a function of both Ω_c and Ω_p. In the EIT domain, characterized by Ω_c, $\Omega_p \lesssim \Gamma_{eg}$ and outlined by the dashed line, the separation between the contour lines decreases as a function of distance from the origin, reflecting that in the EIT regime $\gamma_{\rm EIT} \approx (\Omega_c^2 + \Omega_p^2)/\Gamma_{eg}$. Further out, as the system enters the ATS regime, the separation between the contour lines tends to become fixed. Figure 3(b) shows that in the AT regime, characterized by $\Omega_c \gtrsim \Gamma_{eg}$, the $\gamma_{\rm ATS}$ contour lines are equidistant circles, reflecting the fact that $\gamma_{\rm ATS} \approx \sqrt{\Omega_c^2 + \Omega_p^2}$ in that regime. In figure 3(b), near the x-axis, and in figure 2(c) it is $\Omega_p \ll \Omega_c$ and therefore $\gamma_{\rm ATS} \approx \Omega_c$. These trends for $\gamma_{\rm ATS}$ are also borne out by calculating the separation between the pair of non-dark eigenstates of the (decay-free) Hamiltonian in equation (1), when setting all detunings to zero.

Calculations similar to those shown in figures 2 and 3 can be performed at any atom temperature (see [32] and references therein), and for both cascade and Λ-type three-level atoms. In the hot-atom cases (i.e., in vapor cells), the difference between coupler and probe wavelengths determines the size of residual Doppler shifts, which in turn determines the visibilities and detailed shapes of EIT and ATS spectra. In hot gases $\gamma_{\rm EIT}$ generally tends to be larger than in the cold-atom case, in particular in weak coupler and probe fields, and follows a different scaling (see figure 7 in [32]).

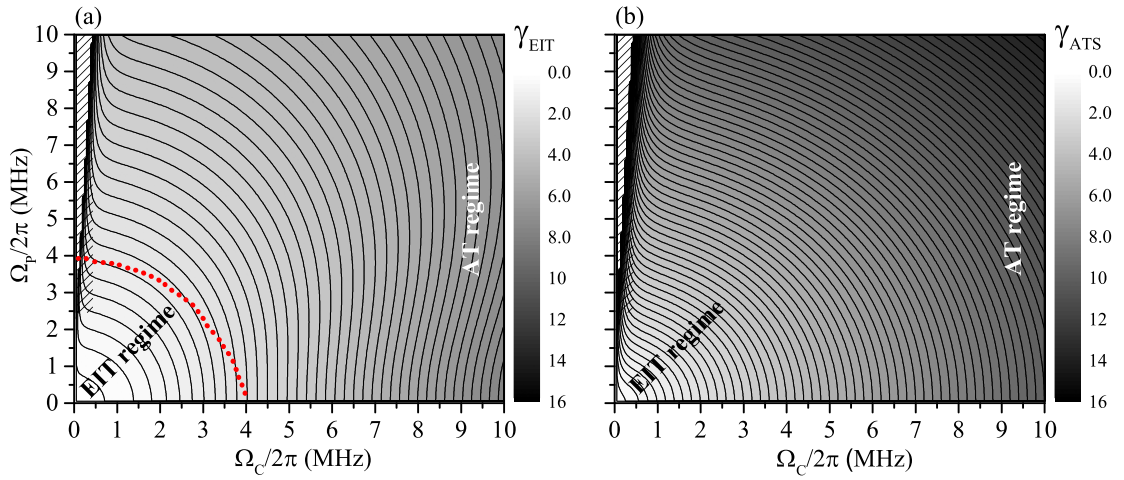

Figure 3. (a) Calculated γ_{EIT} as a function of Ω_p and Ω_c. Within the displayed parameter space, the EIT regime is found in the lower-left corner. In that regime, $\gamma_{EIT} \approx (\Omega_c^2 + \Omega_p^2)/\Gamma_{eg} \lesssim \Gamma_{eg}$. (b) Calculated γ_{ATS} as a function of Ω_p and Ω_c. Except in a region of coupler Rabi frequencies considerably less than Γ_{eg}, it is $\gamma_{ATS} \approx \sqrt{\Omega_c^2 + \Omega_p^2}$.

3. Experimental measurement

The EIT and ATS experiments are performed in a standard MOT with temperature ~100 μK and atomic density up to ~10^{10} cm^{-3}. The coupling and probe lasers have linear and parallel polarizations and counter-propagate through the cold-atom cloud, as seen in figure 1(b). The details of the experiment have been described previously [38]. The probe beam is derived from a diode laser (DLpro, Toptica) that is locked to the ground-state transition, $|1\rangle \rightarrow |2\rangle$, using polarization spectroscopy [39]; the beam has a Gaussian waist $\omega_{p0} = 10$ μm at the MOT center. The strong coupling laser (Toptica TA-SHG110) has a Gaussian waist $\omega_{c0} = 30$ μm and drives the Rydberg transition $|2\rangle \rightarrow |3\rangle$. The frequency of the coupling laser is stabilized to the Rydberg transition using a Rydberg-EIT signal obtained from a cesium room-temperature vapor cell [40]. In each experimental cycle, after turning off the trap beams, we switch on the coupling and probe lasers for 25 μs. During the probe pulse the probe-laser frequency is swept across the $|6S_{1/2}, F = 4\rangle \rightarrow |6P_{3/2}, F' = 5\rangle$ transition using a double-pass acousto-optic modulator (AOM) over a range of ± 10 MHz relative to the transition center.

In order to avoid Rydberg excitation blockade and interaction effects, and to be able to reach high coupling Rabi frequencies, Ω_c, we have chosen a state with a low principal quantum number n ($35S_{1/2}$). Also, the MOT density is reduced to about ~10^8 cm^{-3} by reducing the repumping laser power. Further, to ensure that the effect of radiation pressure [38, 41] on the EIT and ATS spectral profiles is negligible, we use a single-photon counter module (SPCM) for probe-light detection, allowing us to use a very low probe power, $P_{852} = 200$ pW. Under these conditions, the radiation-pressure-induced velocity change during the probe pulse has an upper limit of ≈7 cm s^{-1}, corresponding to Doppler shifts <100 kHz (which is negligible in the present work). The EIT and ATS spectra are recorded using a data acquisition card (NI-PCI-6542) and processed with a Labview program.

The absorption coefficient, α, is obtained from the measured SPCM count number, $P(\Delta_p)$, and the off-resonant (absorption-free) count number, P_0, using the relation $\alpha L = -\ln(P(\Delta_p)/P_0)$, where L is the effective MOT diameter along the probe beam path. In figure 4, we present experimental EIT and ATS sample spectra with indicated linewidth parameters γ_{EIT} and γ_{ATS}. We have determined γ_{EIT} and γ_{ATS} from experimental spectra covering a range of the coupling Rabi frequency Ω_c, for fixed Ω_p. In figure 5 we show the measured (hollow symbols) and calculated (lines) results for γ_{EIT} and γ_{ATS} versus Ω_c.

To compare experimental spectra with calculated ones, it is important to account for the laser linewidth in the model. The utilized diode laser systems exhibit a frequency jitter on the order of 1 MHz FWHM, whereas high-frequency laser phase noise is negligible. The frequency jitter causes inhomogeneous broadening of the spectra, because in every realization of the experiment the lasers have a slightly different frequency, that does not change significantly over the duration of a single realization. To account for the inhomogeneous broadening, subsequent to solving the Master equation and obtaining calculated spectra such as the ones in figure 2, the spectra are convoluted with a Gaussian, whose width is given by the laser-frequency jitter. It is noted that high-frequency laser noise would cause homogeneous broadening, which would have to be accounted for differently, namely via additional dephasing terms in the off-diagonal terms in equation (3). The γ_{EIT} and γ_{ATS}-values are obtained from the convoluted calculated spectra. In the present case, the calculations for 1.5 MHz FWHM of the

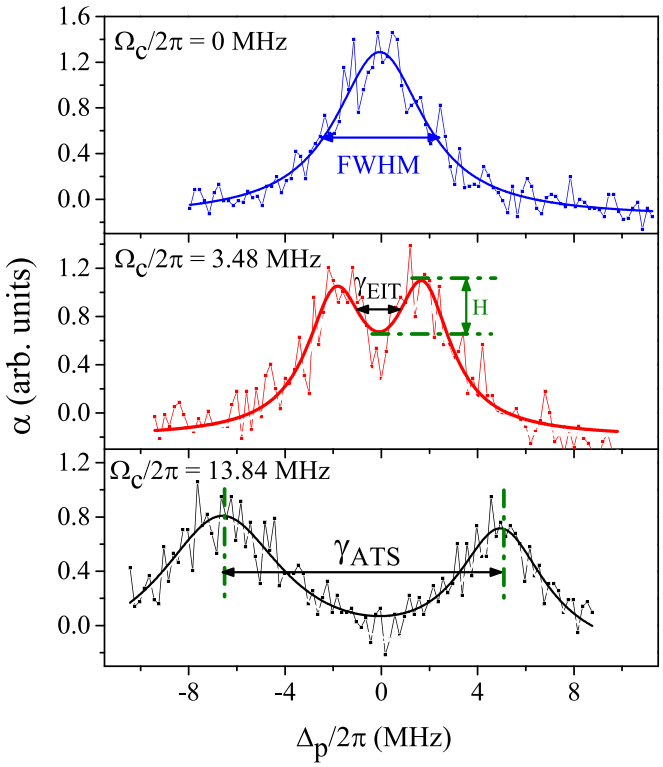

Figure 4. Measurements of EIT and ATS absorption spectra for $\Omega_p = 2\pi \times 1.05$ MHz and the indicated Rabi frequencies of the coupling laser, $\Omega_c = 2\pi \times 0$ MHz (top), 3.48 MHz (middle) and 13.8 MHz (bottom). The solid lines show the results of Lorentzian multi-peak fits. The coupler-free linewidth (top curve) is $2\pi \times (4.5 \pm 0.3)$ MHz, which is close to the expected value of $2\pi \times 5.2$ MHz. The FWHM EIT linewidth, $\gamma_{\rm EIT}$, and the ATS, $\gamma_{\rm ATS}$, are obtained from the fit functions, as indicated. The depth of the EIT dip (or, in the ATS regime, the depth of the valley between the AT peaks), H, is defined as the difference between the peak absorption, averaged over the two peaks, and the absorption minimum between the peaks.

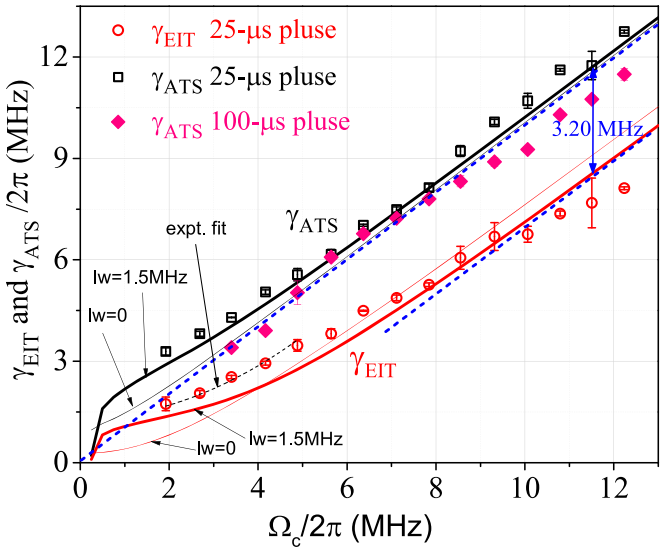

Figure 5. Measurements (symbols) and calculations (solid lines) of $\gamma_{\rm ATS}$ and $\gamma_{\rm EIT}$ as a function of Ω_c for $\Omega_p = 2\pi \times 1.05$ MHz and probe/coupling duration 25 μs (hollow) and 100 μs (filled). In the calculation, the laser linewidth is $2\pi \times 1.5$ MHz (bold solid lines) and 0 (thin solid lines). The black thin dashed line shows a fit to the experimental data; the fit function is $\gamma_{\rm EIT} \approx A + B(\Omega_c^2 + \Omega_p^2)/\Gamma_{eg}$ with $A = 2\pi \times (1.42 \pm 0.10)$ MHz and $B = 0.44 \pm 0.03$.

laser-frequency jitter (bold solid lines in figure 5) reproduce the measurements best (also see discussion of figure 6 below).

We first discuss the EIT linewidth $\gamma_{\rm EIT}$. In the EIT domain, characterized by $\Omega_c, \Omega_p \lesssim \Gamma_{eg}$, the value of $\gamma_{\rm EIT}$ in figure 5 exhibits a quadratic behavior, as expected from figure 3(a). For the experimental data in figure 5, we find

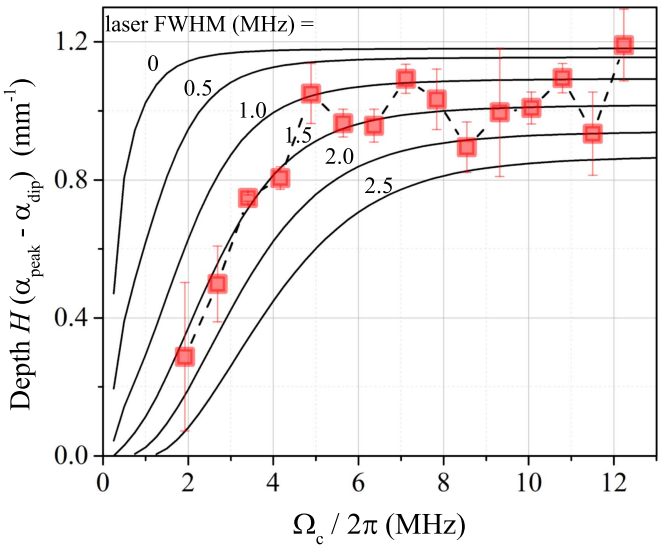

Figure 6. Measurements (symbols) and calculations (black solid lines) of the depth of the transparency window, H, defined in figure 4, versus Ω_c for $\Omega_p = 2\pi \times 1.05$ MHz. The FWHM of the laser jitter in the calculations ranges from 0 to 2.5 MHz. The curve for 1.5 MHz laser linewidth reproduces the experimental data best.

that in the EIT domain the data are fit quite well by an equation $\gamma_{\rm EIT} \approx A + B(\Omega_c^2 + \Omega_p^2)/\Gamma_{eg}$, as shown by the black thin dashed line. The fitting parameters, which are introduced to account for the inhomogeneous line broadening caused by the laser-frequency jitter, are found to be $A = 2\pi \times (1.42 \pm 0.10)$ MHz and $B = 0.44 \pm 0.03$. Without the inhomogeneous broadening, it would be $A \approx 0$ and $B \approx 1$. It is seen that the laser jitter reduces the pre-factor B to a value significantly less than its ideal value of 1, and it adds an additive constant A on the order of the laser linewidth. In the AT regime, characterized by $\Omega_c \gtrsim \Gamma_{eg}$, the $\gamma_{\rm EIT}$-value follows a trend $\gamma_{\rm EIT} \approx \Omega_c - 2\pi \times 3.2$ MHz. (In the absence of laser-line broadening, in the AT regime it would be $\gamma_{\rm EIT} \approx \Omega_c - \Gamma_{eg}/2 = \Omega_c - 2\pi \times 2.6$ MHz). Over the entire Ω_c-range studied, the measured dependence $\gamma_{\rm EIT}(\Omega_c)$ agrees quite well with a calculation in which a Gaussian laser-frequency jitter of 1.5 MHz FWHM is assumed.

Next we discuss $\gamma_{\rm ATS}$. In the AT regime, $\Omega_c \gtrsim \Gamma_{eg}$, and for $\Omega_p \ll \Omega_c$, it is $\gamma_{\rm ATS} \approx \Omega_c$. In the EIT regime, Ω_c, $\Omega_p \lesssim \Gamma_{eg}$, the value of $\gamma_{\rm ATS}$ tends to be larger than Ω_c; for $\Omega_c \lesssim 2\pi \times 2$ MHz $\gamma_{\rm ATS}$ cannot be determined because the spectrum ceases to split into a separated line pair (also see figure 6). Inhomogeneous broadening due to the laser-frequency jitter generally increases the measured $\gamma_{\rm ATS}$, because the outer wings of the split lines are wider than the inside wings, hence the spectral averaging will pull the line centers in figure 2(b) outward. The absorption minimum at $\Delta_p = 0$ disappears entirely when Ω_c drops below a critical value, which is related to the laser linewidth and other broadening mechanisms. In our case this critical value is $\approx 2\pi \times 2$ MHz. Similar nonlinear behavior of the AT splitting is observed in [32], where an RF-induced ATS is used to measure a microwave electric field.

We note that Ω_c has a different significance in the EIT and AT domains. In the AT regime, Ω_c splits the lines but does not broaden them, whereas in the EIT regime Ω_c broadens the EIT line, as $\gamma_{\rm EIT}$ increases with $(\Omega_c^2 + \Omega_p^2)$. Conversely, laser jitter and other inhomogeneous broadening mechanisms also have a different significance in the two domains. In the EIT domain the spectra are very sensitive to inhomogeneous broadening, because even moderate laser jitter already strongly affects the parameters A and B in the fit function $\gamma_{\rm EIT} \simeq A + B(\Omega_c^2 + \Omega_p^2)/\Gamma_{eg}$. (In the absence of broadening, it would be $A = 0$ and $B = 1$.) In the ATS domain, the broadening has a comparatively small effect on $\gamma_{\rm EIT}$, and an even smaller one on $\gamma_{\rm ATS}$. Generally, the agreement between theory and experiment in figure 5 is slightly better for $\gamma_{\rm ATS}$ than it is for $\gamma_{\rm EIT}$. We believe this is because the details of the line broadening are harder to model than the AT splitting of the line centers.

In figure 5 we have included a similar measurement with 100 μs probe- and coupler-pulse sweeps (filled diamonds in figure 5). It is seen that $\gamma_{\rm ATS}$ for the longer pulses is less than in the 25 μs case. We attribute the reduction in $\gamma_{\rm ATS}$ in part to dephasing caused by Rydberg-atom interactions, which could be considered via the dephasing terms in equation (3). Longer pulses will generally lead to a higher Rydberg-atom number in the atom-field interaction volume, causing dephasing by Rydberg–Rydberg interactions. The dependence of the ATS splitting on Rydberg interactions is detailed in [26]; in our present work interactions are avoided by using a low principal quantum number, a low atom density and a relatively short interaction time. Longer times will also increase the likelihood of Penning and thermal ionization. Any ions in the sample would contribute to Rydberg-level dephasing via the ion electric fields. With increasing pulse duration, the spectra are also increasingly

affected by radiation-pressure-induced Doppler shifts, causing changes in the γ_{ATS}-values derived from the spectra.

We finally consider the depth of the transparency window, which is an important measure for any practical application of EIT and ATS. The depth of the transparency window, H, is defined as the difference between the absorption coefficients on the peaks and at the center of the spectrum, $\Delta_p = 0$ (see middle curve in figure 4). The depth H increases with Ω_c in the EIT regime and plateaus at a laser-jitter-dependent maximal value in the ATS regime, as shown by the calculated curves in figure 6. Assuming a laser jitter with 1.5 MHz FWHM, we achieve good agreement between experiment and calculation. This best-fit laser linewidth agrees well with manufacturer estimates for the utilized laser systems.

4. Conclusion

We have presented measured and calculated cold-atom EIT and AT absorption spectra of a cascade three-level atom involving the $35S_{1/2}$ Rydberg state. The measurements show good agreement with calculations. The spectra exhibit two regimes, an EIT regime for weak Ω_c and Ω_p, and an ATS regime for large Ω_c. While similar in appearance, the EIT and AT spectra are different in physical interpretation [9, 10]. We have defined widths γ_{EIT} and γ_{ATS} that facilitates making the distinction between EIT and ATS. In the cold-atom EIT regime, Ω_c, $\Omega_p \lesssim \Gamma_{eg}$, we find $\gamma_{EIT} = A + B((\Omega_c^2 + \Omega_p^2)/\Gamma_{eg})$, where the parameters A and B depend on inhomogeneous broadening due to laser jitter. The MOT magnetic field, which is always left on, may add to the inhomogeneous broadening. In the ATS regime, $\Omega_c \gtrsim \Gamma_{eg}$, it is $\gamma_{ATS} \approx \Omega_c$ and $\gamma_{EIT} = \gamma_{ATS} - C$, with a constant $C \gtrsim \Gamma_{eg}/2$. The lower limit of C is realized in the absence of inhomogeneous broadening. An emphasis of our analysis has been to include the effects of laser jitter, saturation of the probe transition, and Doppler mismatch caused by non-zero temperature and unequal probe and coupling laser wavelengths.

Practical criteria to distinguish between EIT and ATS, as developed in this work, are valuable in a wide variety of atomic-physics, quantum-optics and quantum information applications of these schemes. For instance, the details of ATS splitting and line broadening effects are important in applications that deal with quantitative, atom-based microwave field measurements using Rydberg-EIT and microwave-coupled ATS [27, 32]. Cold-atom, narrow-linewidth EIT and ATS are helpful in improving the accuracy and resolution of the atom-based field measurements.

Acknowledgments

The work was supported by the National Key R&D Program of China (Grant No. 2017YFA0304203), the National Natural Science Foundation of China (Grants No. 61475090, and No. 61675123, and No. 61775124), Changjiang Scholars and Innovative Research Team in University of Ministry of Education of China (Grant No. IRT13076), the State Key Program of National Natural Science of China (Grant No. 11434007) and 1331 KSC. GR acknowledges support by the NSF (PHY-1506093) and BAIREN plan of Shanxi province.

References

[1] Boller K J, Imamoğlu A and Harris S E 1991 *Phys. Rev. Lett.* **66** 2593–6
[2] Hau L V, Harris S E, Dutton Z and Behroozi C H 1999 *Nature* **397** 594
[3] Phillips D F, Fleischhauer A, Mair A, Walsworth R L and Lukin M D 2001 *Phys. Rev. Lett.* **86** 783
[4] Autler S H and Townes C H 1955 *Phys. Rev.* **100** 703
[5] Xiao M, Li Y, Jin S and Gea-Banacloche J 1995 *Phys. Rev. Lett.* **74** 666
[6] Scully M O and Zubairy M S 1997 *Quantum Optics* (Cambridge: Cambridge University Press)
[7] Fleischhauer M, Imamoglu A and Marangos J P 2005 *Rev. Mod. Phys.* **77** 633
[8] Weatherill K J, Pritchard J D, Abel R P, Bason M G, Mohapatra A K and Adams C S 2008 *J. Phys. B: At. Mol. Opt. Phys.* **41** 201002
[9] Abi-Salloum T Y 2010 *Phys. Rev.* A **81** 053836
[10] Anisimov P M, Dowling J P and Sanders B C 2011 *Phys. Rev. Lett.* **107** 163604
[11] Peng B, Özdemir S K, Chen W, Nori F and Yang L 2014 *Nat. Commun.* **5** 5082
[12] Lu X, Miao X, Bai J, Yuan Y, Wu L, Fu P, Wang R and Zuo Z 2015 *Chin. Phys.* B **24** 094204
[13] Lu X, Miao X, Bai J, Pei L, Wang M, Gao Y, Wu L A, Fu P, Wang R and Zuo Z 2015 *J. Phys. B: At. Mol. Opt. Phys.* **48** 055003
[14] Zhang X, Wu S and Li H 2017 *Commun. Theor. Phys.* **67** 217–21
[15] Mohapatra A K, Jackson T R and Adams C S 2007 *Phys. Rev. Lett.* **98** 113003
[16] Pritchard J D, Maxwell D, Gauguet A, Weatherill K J, Jones M P A and Adams C S 2010 *Phys. Rev. Lett.* **105** 193603
[17] Gorniaczyk H, Tresp C, Schmidt J, Fedder H and Hofferberth S 2014 *Phys. Rev. Lett.* **113** 053601
[18] Dudin Y and Kuzmich A 2012 *Science* **336** 887–9
[19] Viscor D, Li W and Lesanovsky I 2015 *New J. Phys.* **17** 033007
[20] Singer K, Reetz-Lamour M, Amthor T, Marcassa L and Weidemüller M 2004 *Phys. Rev. Lett.* **93** 163001
[21] Tong D, Farooqi S, Stanojevic J, Krishnan S, Zhang Y, Côte R, Eyler E and Gould P 2004 *Phys. Rev. Lett.* **93** 063001
[22] Vogt T, Viteau M, Zhao J, Chotia A, Comparat D and Pillet P 2006 *Phys. Rev. Lett.* **97** 083003

[23] Teo B K, Feldbaum D, Cubel T, Guest J R, Berman P R and Raithel G 2003 *Phys. Rev.* A **68** 053407
[24] DeSalvo B J, Aman J A, Gaul C, Pohl T, Yoshida S, Burgdörfer J, Hazzard K R A, Dunning F B and Killian T C 2016 *Phys. Rev.* A **93** 022709
[25] Zhang H, Wang L M, Chen J, Bao S, Zhang L, Zhao J and Jia S 2013 *Phys. Rev.* A **87** 033835
[26] Zhang H, Zhang L, Wang L, Bao S, Zhao J, Jia S and Raithel G 2014 *Phys. Rev.* A **90** 043849
[27] Sedlacek J A, Schwettmann A, Kübler H, Löw R, Pfau T and Shaffer J P 2012 *Nat. Phys.* **8** 819
[28] Sedlacek J A, Schwettmann A, Kübler H and Shaffer J P 2013 *Phys. Rev. Lett.* **111** 063001
[29] Holloway C L, Gordon J A, Schwarzkopf A, Anderson D A, Miller S A, Thaicharoen N and Raithel G 2014 *Appl. Phys. Lett.* **104** 244102
[30] Anderson D A, Schwarzkopf A, Miller S A, Thaicharoen N, Raithel G, Gordon J A and Holloway C L 2014 *Phys. Rev.* A **90** 043419
[31] Jiao Y, Hao L, Han X, Bai S, Raithel G, Zhao J and Jia S 2017 *Phys. Rev. Appl.* **8** 014028
[32] Holloway C L, Simons M T, Gordon J A, Dienstfrey A, Anderson D A and Raithel G 2017 *J. Appl. Phys.* **121** 233106
[33] Nie Z Q, Zhang H B, Li P Z, Yang Y M, Zhang Y P and Xiao M 2008 *Phys. Rev.* A **77** 063829
[34] Zhang Z Y, Zheng H B, Yao X, Tian Y L, Che J L, Wang X X, Zhu D Y, Zhang Y P and Xiao M 2015 *Sci. Rep.* **5** 10462
[35] Che J L, Zhang Y Q, Zhang Y F, Liu J, Cheng Q Y and Zhang Y P 2016 *J. Phys. B: At. Mol. Opt. Phys.* **49** 174002
[36] Che J L, Zhang Z Y, Hu M L, Shi X W and Zhang Y P 2018 *Opt. Exp.* **26** 3054
[37] Raitzsch U, Heidemann R, Weimer H, Butscher B, Kollmann P, Löw R, Büchler H P and Pfau T 2009 *New J. Phys.* **11** 055014
[38] Jiao Y, Han X, Yang Z, Zhao J and Jia S 2016 *Chin. Phys. Lett.* **33** 123201
[39] Pearman C P, Adams C S, Cox S G, Griffin P F, Smith D A and Hughes I G 2002 *J. Phys. B: At. Mol. Opt. Phys.* **35** 5141–51
[40] Jiao Y, Li J, Wang L, Zhang H, Zhang L, Zhao J and Jia S 2016 *Chin. Phys.* B **25** 053201
[41] Bai S, Han X, Jiao Y, Hao L, Zhao J and Jia S 2017 *J. Mod. Phys.* **8** 1884–93